

Accurate and efficient simulation of photoemission spectroscopy via Kohn-Sham scattering states

Gian Parusa,^{1,2,3} Sotirios Fragkos,⁴ Samuel Beaulieu,⁴ and Michael Schüler^{1,2,3}

¹*PSI Center for Scientific Computing, Theory and Data,
Paul Scherrer Institute, 5232 Villigen PSI, Switzerland*

²*Department of Physics, University of Fribourg, 1700 Fribourg, Switzerland*

³*National Centre for Computational Design and Discovery of Novel Materials (MARVEL),
Paul Scherrer Institute, 5232 Villigen PSI, Switzerland*

⁴*Université de Bordeaux—CNRS—CEA, CELIA, UMR5107, F33405 Talence, France*

(Dated: January 21, 2026)

We introduce an efficient first-principles framework for simulating angle-resolved photoemission spectroscopy (ARPES) by computing photoelectron states as solutions of the Kohn–Sham equation with scattering boundary conditions. This approach is formally equivalent to the Lippmann–Schwinger formalism but offers superior computational efficiency and direct integration with plane-wave or real-space density functional theory. By enabling direct calculation of photoemission matrix elements, our method bridges the gap between intrinsic electronic properties and experimental ARPES spectra. We demonstrate its accuracy through circular dichroism ARPES simulations for monolayer graphene and bulk 2H-WSe₂, achieving excellent agreement with experimental data and highlighting the critical role of pseudopotentials in describing high-energy photoelectron scattering. Our results establish a robust and accessible route for quantitative ARPES modeling, paving the way for advanced studies of orbital textures, many-body effects, and time-resolved photoemission.

Introduction.— ARPES is one of the most powerful experimental techniques to probe the electronic structure of solids [1–4]. The inherent conservation of crystal momentum in the photoemission process enables ARPES to map the occupied band structure, providing direct insights into the Fermi surface, band topology, surface states, and many-body interactions in materials. Periodic solids are, however, more than just their band structure, as the momentum-dependent orbital character and complex-valued electronic wavefunctions also play a crucial role in determining their physical properties. Paradigmatic examples include the orbital texture in transition metal dichalcogenides [5–7], topological insulators [8–12], Weyl semimetals [13–17] and beyond [18, 19].

Such wavefunction information is encoded in the ARPES intensity via the photoemission matrix elements, which describe the transition from an initial Bloch state to a final photoelectron state upon interaction with light. It is generally believed that circular dichroism in ARPES (CD-ARPES) is sensitive to the orbital angular momentum and Berry curvature of the initial states [20–25]. On the other hand, ARPES is sensitive to details of the final photoelectron states. In particular, the experimental geometry has a profound impact on the ARPES intensity and circular dichroism patterns [26], while various intra-atomic and inter-atomic scattering channels can contribute to the final photoelectron states. The interplay of these contributions leads to complex photon-energy dependent interference effects. Additionally, multiple scattering of the photoelectron wavefunctions in the crystal potential can have a profound impact [27, 28]. As a result, there is a gap between the intrinsic, i.e., measurement-independent properties of the initial states and the experimentally observed ARPES spectra.

To bridge this gap, accurate simulation tools of ARPES spectra are essential. Besides model approaches based on (ab initio) tight-binding Hamiltonians that can already reveal the impact of interference effects [29, 30], several first-

principle methods have been put forward. The most prominent ones include time-dependent density functional theory (TDDFT) [31–33] and multiple scattering theory based on the Korringa–Kohn–Rostoker (KKR) method [34]. While these methods have achieved significant success in predicting ARPES spectra, they often require substantial computational resources and may not directly yield the photoemission matrix element directly, needed to disentangle intrinsic and extrinsic contributions in the spectra. The direct calculation of the final photoelectron states using the theory of time-reversed low-energy electron diffraction (trLEED) [35–37] or high-energy Bloch states [38] has been used by few groups, but so far not widely adopted in the community. Ryoo and Park have recently demonstrated how to compute trLEED states through the Lippmann–Schwinger (LS) equation [39], narrowing the gap between standard density functional theory (DFT) implementations and ARPES simulations.

In this work, we present an alternative approach to compute the final photoelectron states by directly solving the Kohn–Sham equation with appropriate boundary conditions. We show that this approach is fully equivalent to the LS formalism, directly compatible with standard plane-wave DFT implementations, and significantly more efficient. We also investigate a key aspect of ARPES simulations in the context of plane-wave or real-space DFT, namely the use of pseudopotentials to represent the ionic potential. While pseudopotentials are widely used in ground-state DFT calculations, their accuracy for describing high-energy photoelectron states is less clear. We analyze the impact of different pseudopotentials on the computed ARPES spectra and circular dichroism patterns, demonstrating that high-quality pseudopotentials enable accurate ARPES simulations up to the soft X-ray photon regime. As concrete examples, we focus on monolayer graphene and bulk 2H-WSe₂ and compare the predicted spectra to published experimental data and new experimental measurements. Our work

establishes a robust and efficient framework for first-principles ARPES simulations – to be supported by an upcoming open-source implementation – that can be widely adopted by the community.

Theory.— Under the sudden approximation, the dipole approximation, and under the assumption of sharp quasiparticle peaks, the ARPES intensity can be expressed as [40],

$$I(\mathbf{k}, E) = \sum_{\alpha} f_{\alpha}(\mathbf{k}) |\hat{e} \cdot \mathcal{M}_{\alpha}(\mathbf{k}, E)|^2 \delta(\varepsilon_{\alpha}(\mathbf{k}) + \hbar\omega - E).$$

Here, $f_{\alpha}(\mathbf{k})$ is the occupation function of the Bloch state $|\psi_{\mathbf{k}\alpha}\rangle$ with band index α and crystal momentum \mathbf{k} , $\varepsilon_{\alpha}(\mathbf{k})$ is its corresponding energy, ω is the photon energy, E is the photoelectron energy, \hat{e} is the polarization vector of light, and $\mathcal{M}_{\alpha}(\mathbf{k}, E)$ is the photoemission matrix element. It is defined as

$$\mathcal{M}_{\alpha}(\mathbf{k}, E) = \langle \chi_{\mathbf{p}} | \hat{\Delta} | \psi_{\mathbf{k}\alpha} \rangle, \quad (1)$$

where $\hat{\Delta}$ is the light-matter coupling operator, and $|\chi_{\mathbf{p}}\rangle$ is the final state with momentum \mathbf{p} and energy $E = \mathbf{p}^2/2$. In-plane momentum conservation implies $\mathbf{p} = \mathbf{k} + \mathbf{p}_{\perp} \hat{\mathbf{z}}$ with $\hat{\mathbf{z}}$ being the surface normal direction.

Both the initial Bloch states and the final photoelectron states can be obtained from the Kohn-Sham (KS) equation $\hat{H}^{\text{KS}}|\psi\rangle = \varepsilon|\psi\rangle$. To clarify, we assume a two-dimensional periodic system [41]. Building on previous works [42–46], we employ the in-plane Laue representation for wavefunctions:

$$\phi_{\mathbf{k}}(\mathbf{r}) = \sum_{\mathbf{G}} e^{i(\mathbf{k}+\mathbf{G}) \cdot \mathbf{r}_{\parallel}} f_{\mathbf{k},\mathbf{G}}(z). \quad (2)$$

For the mixed plane-wave/real-space function $f_{\mathbf{k},\mathbf{G}}(z)$, the KS equation becomes

$$\sum_{\mathbf{G}'} [\hat{T}_{\mathbf{G}\mathbf{G}'} + \hat{V}_{\mathbf{G}\mathbf{G}'}] f_{\mathbf{k},\mathbf{G}'}(z) = \varepsilon f_{\mathbf{k},\mathbf{G}}(z), \quad (3)$$

where

$$\hat{T}_{\mathbf{G}\mathbf{G}'} = \left(\frac{1}{2}(\mathbf{k} + \mathbf{G})^2 - \frac{1}{2} \frac{d^2}{dz^2} \right) \delta_{\mathbf{G}\mathbf{G}'} \quad (4)$$

is the kinetic energy operator, and $\hat{V}_{\mathbf{G}\mathbf{G}'}$ is the KS potential in Laue representation.

The key distinction of the final states from the initial states lies in the boundary conditions. Bound states obey $f_{\mathbf{k},\mathbf{G}}(z) \rightarrow 0$ as $z \rightarrow \pm\infty$, rendering Eq. (3) an eigenvalue problem. In contrast, the final states behave as $f_{\mathbf{k},\mathbf{G}}(z) = e^{ip_{\perp}z} + r_{\mathbf{k},\mathbf{G}} e^{-ik(\mathbf{G})z}$ as $z \rightarrow +\infty$, and $f_{\mathbf{k},\mathbf{G}}(z) = t_{\mathbf{k},\mathbf{G}} e^{ik(\mathbf{G})z}$ as $z \rightarrow -\infty$, where $\kappa(\mathbf{G}) = \sqrt{2E - (\mathbf{k} + \mathbf{G})^2}$, and $r_{\mathbf{k},\mathbf{G}}$ and $t_{\mathbf{k},\mathbf{G}}$ are unknown coefficients. Only kinematically allowed channels with $2E > (\mathbf{k} + \mathbf{G})^2$ – in the language of multi-channel scattering theory [47], open channels – contribute to the asymptotic behavior [48]. Just like in multi-channel scattering theory [49], the asymptotic boundary conditions transform the KS equation (3) into a linear equation for $f_{\mathbf{k},\mathbf{G}}(z)$ [50].

Multi-channel scattering theory also establishes a direct link to the LS formalism employed in Ref. [39]. Treating the kinetic energy (4) as matrix $\hat{\mathbf{T}}$ in \mathbf{G} -space, one can readily define the Green's function of the ordinary differential equation $[\mathbf{E}\mathbf{I} - \hat{\mathbf{T}}]\mathbf{K}(E; z, z') = \mathbf{I}\delta(z - z')$. Since $\hat{\mathbf{T}}$ is diagonal in \mathbf{G} -space, the Green's function is also diagonal with elements

$$K_{\mathbf{G}}(E; z, z') = -\frac{1}{\alpha_{\mathbf{G}}(E)} e^{-\alpha_{\mathbf{G}}(E)|z-z'|}. \quad (5)$$

Here, $\alpha_{\mathbf{G}}(E) = \sqrt{(\mathbf{k} + \mathbf{G})^2 - 2E}$ for closed channels and $\alpha_{\mathbf{G}}(E) = i\kappa(\mathbf{G})$ for open channels. Using this Green's function, one can rewrite Eq. (3) into the LS equation,

$$f_{\mathbf{k},\mathbf{G}}(z) = e^{ip_{\perp}z} \delta_{\mathbf{G},0} + \sum_{\mathbf{G}'} \int dz' K_{\mathbf{G}}(E; z, z') \times (\hat{V}_{\mathbf{G}\mathbf{G}'} f_{\mathbf{k},\mathbf{G}'})(z'). \quad (6)$$

In practical terms, both the LS equation (6) and the KS equation (3) with scattering boundary conditions are solved on a discrete z -grid with grid spacing h , transforming them to linear systems of equations; given a typical problem size, iterative linear solvers are employed. We have implemented both approaches with higher-order discretization up to $\mathcal{O}(h^5)$ and verified their numerical equivalence [50]. However, the route via the KS equation offers the advantage of highly effective preconditioning strategies akin to those used in iterative diagonalization, leading to significantly faster convergence.

Results.— To demonstrate the capabilities of our method, we present theoretical ARPES results obtained by solving the KS equations for monolayer graphene and bulk 2H-WSe₂ and compare them with published [51] and new experimental data. In particular, we focus on dichroism as the key observable. In particular, the circular dichroism in the angular distribution (CDAD) is highly sensitive to the detailed structure of the final states, making it a stringent and well-suited benchmark for assessing the accuracy of our approach.

For graphene, we compare our theoretical method against the experimental results from Ref. [51] and adopt the same experimental geometry as illustrated in Fig. 1(a). The calculations are performed using both all-electron (AE) and pseudopotential (PP) methods [50]. As in Ref. [51], we focus on the CDAD close to the K -point of graphene (see Fig. 1(b)), and we present results for the energy-integrated CDAD normalized to the total intensity. Fig. 1(c) and (d) show the results for photon energies 52 eV and 65 eV, respectively. In Fig. 1(c), we successfully reproduce the nodal line (where the CDAD spectrum vanishes) along the $\Gamma - K$ direction as well as the overall CDAD texture. There are, however, more pronounced "leg" features in the calculation as compared to the experiment. In Fig. 1(d), we also reproduce the $\Gamma - K$ nodal line as well as the other two nodal lines on the first and second quadrants. The overall texture is in remarkable agreement with the experiment. Results for additional photon energies are presented in the Supplementary Material [50]. We also analyzed the maximum intensity of the normalized CDAD as a function

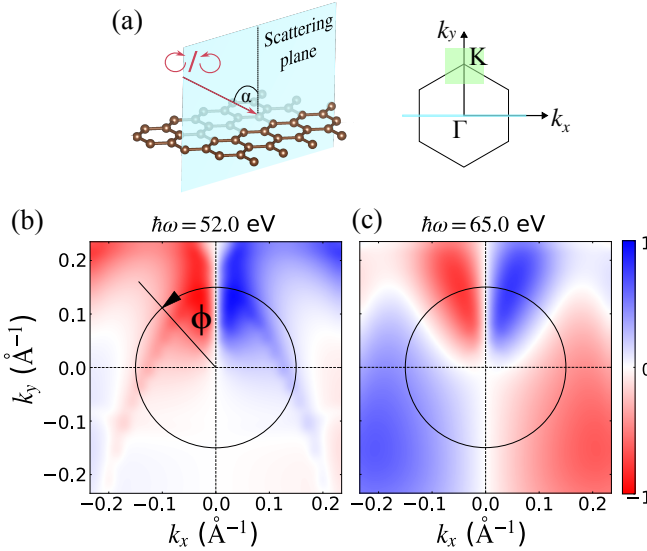


FIG. 1. (a) Experimental geometry used in Ref. [51]. The angle of incidence is $\alpha = 50^\circ$. (b) Sketch of the Brillouin zone of graphene with the region of interest highlighted in green around the K -point. (c) Calculated energy-integrated normalized CDAD around the K -point of graphene at photon energy 52 eV, and (d) at photon energy 65 eV. Results are obtained with all-electron method.

of photon energy, following the same convention as Fig. 2(b) of Ref. [51]. Our results are shown in Fig. 2(a) together with the experimental data. We successfully reproduce the reduction of the maximum intensity at 45 eV as well as the CDAD sign reversal at 75 eV, improving significantly over the KKR results also presented in Ref. [51].

So far, we have used the AE method to compute the photoelectron states. For practical applications, however, PP methods are more widely used due to their efficiency. We now analyze the accuracy of PP methods for simulating ARPES spectra by comparing them to the AE results. We use the generalized norm-conserving PP from the PSEUDODOJO library [52]. The photon-energy-dependent CDAD maximum intensity from PP is also shown in Fig. 2(a). We observe an overall excellent agreement with the AE results over the whole photon energy range. In Fig. 2(b), we compare the methods in more detail by analyzing the normalized CDAD along a circle of radius $r = 0.15 \text{ \AA}^{-1}$ around the K -point, as illustrated in Fig. 1(c). The results for PP agree well with those of AE up to photon energy 100 eV; small deviations start to appear at 65 eV. Nevertheless, the PP results successfully reproduce all the AE features, including the nodal line positions. The success of the PP method can be attributed to its non-local part, which by construction is optimized to reproduce the atomic AE scattering properties [53].

The non-local part of the PP is indeed crucial for reproducing the scattering properties of the photoelectron states. In general, the observed spectra change drastically when one switches off this contribution in the photoelectron state calculation [50]. However, for a photon energy of 52 eV, the dif-

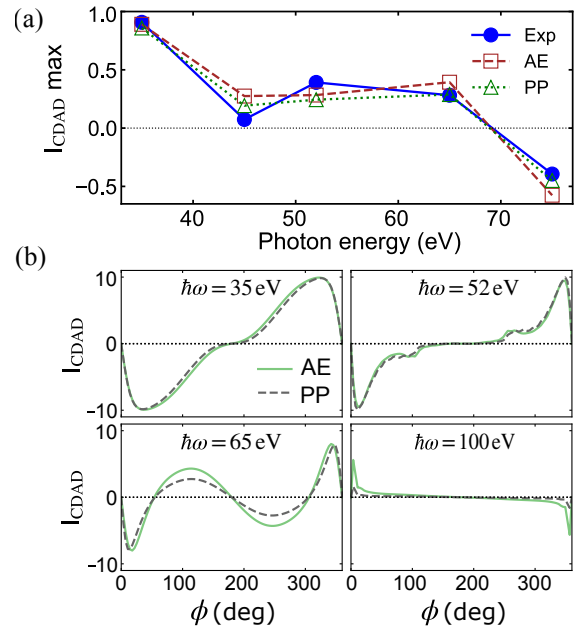


FIG. 2. (a) Comparison of the maximum intensity of the normalized CDAD at the Fermi level along $k_y = 0$ from the experiments, all-electron (AE) and pseudopotential (PP) methods. The experimental data are extracted from Ref. [51], with minus sign indicating CDAD sign reversal. (b) Angular dependence of the normalized CDAD spectra for different photon energies. The angle ϕ is defined in Fig. 1(b).

ference between including and excluding the non-local part is negligible. This is because the final states are predominantly composed of d -like partial waves around the Carbon atoms, which are not affected by the non-local part of the PP that only acts on s and p angular momentum channels [54]. In contrast, non-local contributions to the light-matter coupling operator $\hat{\Delta}$ [55] are negligible in all cases [50].

As a second example, we present new experimental and theoretical results for bulk 2H-WSe₂. The 2H-WSe₂ experimental data have been acquired using the time- and polarization-resolved extreme ultraviolet momentum microscope instrument [56] at the Centre Lasers Intenses et Applications, in Bordeaux, France. Details about the experimental setup can be found elsewhere [56] and in Ref. [50]. The experimental geometry is shown in Fig. 3(a). All calculations are performed with PP method. To highlight the importance of the non-local part of the PP, we compare two variants of PPs: (i) including the semicore states ($5s, 5p$) for W and $3d$ for Se, and (ii) excluding them.

As the first test, we compute the ARPES spectra with p -polarized light and analyze the dark corridor at binding energies close to the valence band maximum. Our calculations [50] with both PP variants reproduce the experimental spectra well, including the rotation of the dark corridor upon crystal rotation by 60° . Taking the difference of the normalized spectra at 0° and 60° crystal rotation defines the time-reversal dichroism in angular distribution (TRDAD) [57]. The TRDAD obtained from experiments (Fig. 3(b), (c)) is in excellent agreement with

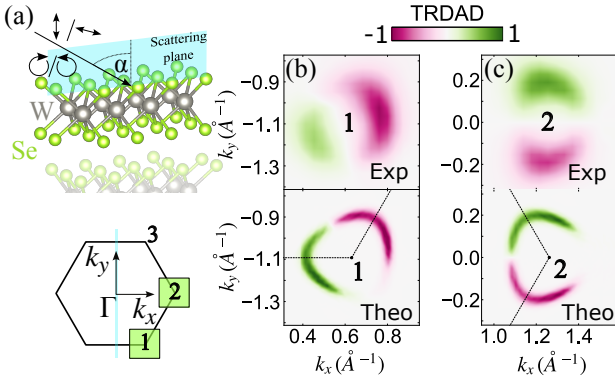


FIG. 3. (a) Experimental geometry for WSe₂. In real space (top panel), the scattering plane is indicated by the vertical plane while in the reciprocal space (bottom panel) it is indicated by the vertical line along the the k_y direction. The angle of incidence is $\alpha = 65^\circ$. (b)–(c) show the TRDAD spectra of the experiment and the theory with $E - E_{\text{VBM}} = -0.25$ eV in the vicinity of K-points 1 and 2, respectively.

our simulations (Fig. 3(d), (e)).

Next we inspect the CDAD, shown in Fig. 3(a) at binding energy $E - E_{\text{VBM}} = -0.25$ eV. We note that PP method with semicore states successfully reproduces the CDAD texture at K -point 2 and 3. This is already different for the PP without semicore states, which only agrees at K -point 3.

For a quantitative comparison, we analyze the valley-integrated CDAD (valley CDAD) at each K -point, which is generally a more robust observable than the full angular distribution. The valley CDAD, presented in Fig. 3(g)–(i) as function of the binding energy, obtained with PP method with semicore states is in almost quantitative agreement with the experiment for all three K -points (note that the experimental and calculated data are normalized the same way). In contrast, the valley CDAD from PP without semicore states deviates from the experiment, especially at K -point 1 and 2, where the valley CDAD of K -point 2 appears to be significantly lower than that of the experiment and thus appears below that of K -point 1. This analysis confirms that including semicore states in the PP is essential for accurately describing the scattering phase of the photoelectron states around each atomic site, which in turn determines the angular distribution through the interferometric nature of the photoemission process [6, 10, 58–61].

Discussion.— In summary, we have presented a method to compute the final photoelectron states by solving the Kohn-Sham equation with appropriate scattering boundary conditions. This approach is fully equivalent to the Lippmann-Schwinger formalism, but significantly more efficient due to the possibility of employing effective preconditioning strategies from iterative diagonalization. We demonstrated that the PP method can accurately describe photoelectron states, provided the pseudoatomic scattering phase matches the AE one. Recent developments of high-accuracy PPs [62] are encouraging in this regard.

In contrast to other methods that yield the photoemission

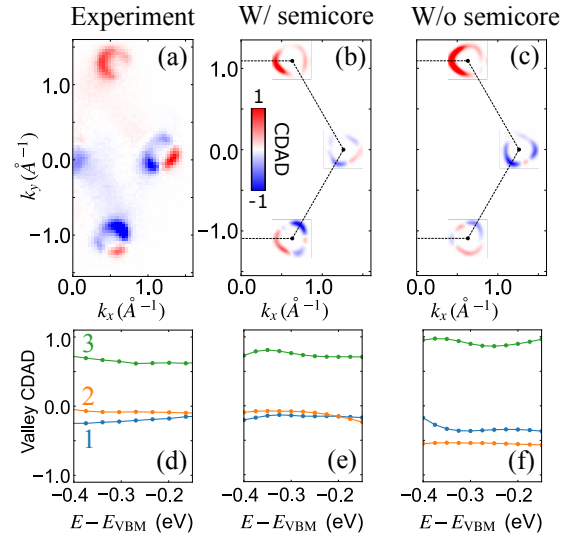


FIG. 4. (a)–(c) CDAD texture at binding energy $E - E_{\text{VBM}} = -0.25$ eV. The spectrum is antisymmetric with respect to the scattering plane and thus only half of the Brillouin zone is shown. (d)–(f) valley-integrated CDAD as a function of binding energy for the experiment, PP with and without semicore states, respectively.

intensity only, calculating the photoelectron states $|\chi_{\mathbf{p}}\rangle$ from the Kohn-Sham equation explicitly offers a number of advantages: (i) the role of multiple scattering and interference effects in the final states can be directly analyzed, (ii) the matrix elements can be computed for arbitrary experimental geometries and light polarizations as post-processing, and (iii) the intrinsic properties of the initial states can be disentangled from extrinsic effects related to the final states. In combination with the direct compatibility with standard DFT, the presented methodology can greatly facilitate the interpretation of ARPES experiments and the fingerprint of orbital textures.

Computing the photoemission matrix elements $\mathcal{M}_{\alpha}(\mathbf{k}, E)$ for the entire relevant band manifold also paves the way an *ab initio* description of ARPES beyond DFT. For instance, the Green's function $G_{\alpha\alpha'}^<(\mathbf{k}, \omega)$ obtained from a *GW* calculation [63] defines the ARPES intensity via $I(\mathbf{k}, E) \propto \sum_{\alpha\alpha'} \mathcal{M}_{\alpha}(\mathbf{k}, E) G_{\alpha\alpha'}^<(\mathbf{k}, \omega - E) \mathcal{M}_{\alpha'}^*(\mathbf{k}, E)$. Similarly, combining Green's function computed from dynamical mean-field theory (typically expressed in Wannier basis m) with $\mathcal{M}_m(\mathbf{k}, E)$ enables a direct experiment-theory comparison for correlated materials.

Finally, *ab initio* description of pump-probe time-resolved ARPES (trARPES) is also possible [64]. The standard formulation of trARPES [65, 66] in language of the time-dependent Green's function requires the photoemission matrix elements for a full description. We have demonstrated the predictive power of this approach for Floquet states in light-driven graphene in Ref. [50] under pump-probe conditions as in recent experiments [67, 68].

The direct calculation of photoelectron states and matrix elements in an efficient and accessible framework is thus a major

step towards the interpretation of ARPES and understanding of materials in and out of equilibrium.

Acknowledgments.— This research was supported by the NCCR MARVEL, a National Centre of Competence in Research, funded by the Swiss National Science Foundation (grant number 205602).

[1] B. Lv, T. Qian, and H. Ding, *Nature Reviews Physics* **1**, 609 (2019).

[2] H. Yang, A. Liang, C. Chen, C. Zhang, N. B. M. Schroeter, and Y. Chen, *Nature Reviews Materials* **3**, 341 (2018).

[3] F. Boschini, M. Zonno, and A. Damascelli, *Rev. Mod. Phys.* **96**, 015003 (2024).

[4] J. A. Sobota, Y. He, and Z.-X. Shen, *Rev. Mod. Phys.* **93**, 025006 (2021).

[5] J. Schusser, H. Orio, M. Ünzelmann, J. Heßdörfer, M. P. T. Masilamani, F. Diekmann, K. Rossnagel, and F. Reinert, *Communications Physics* **7**, 270 (2024).

[6] T. Heider, G. Bihlmayer, J. Schusser, F. Reinert, J. Minár, S. Blügel, C. M. Schneider, and L. Plucinski, *Physical Review Letters* **130**, 146401 (2023).

[7] S. Beaulieu, M. Schüler, J. Schusser, S. Dong, T. Pincelli, J. Maklar, A. Neef, F. Reinert, M. Wolf, L. Rettig, J. Minár, and R. Ernstorfer, *npj Quantum Materials* **6**, 93 (2021).

[8] Y. H. Wang, D. Hsieh, D. Pilon, L. Fu, D. R. Gardner, Y. S. Lee, and N. Gedik, *Physical Review Letters* **107**, 207602 (2011).

[9] H. Bentmann, H. Maaß, E. E. Krasovskii, T. R. F. Peixoto, C. Seibel, M. Leandersson, T. Balasubramanian, and F. Reinert, *Physical Review Letters* **119**, 106401 (2017).

[10] I. Sidilkover, Y. Yen, S. W. D'Souza, J. Schusser, A. Pulkkinen, C. R. Rotundu, M. Hashimoto, D. Liu, Z.-X. Shen, J. Minár, M. Schüler, H. Soifer, and J. A. Sobota, *Physical Review Research* **7**, 033027 (2025).

[11] Y. Wang and N. Gedik, *physica status solidi (RRL) – Rapid Research Letters* **7**, 64 (2013).

[12] H. Bentmann, H. Maaß, J. Braun, C. Seibel, K. A. Kokh, O. E. Tereshchenko, S. Schreyeck, K. Brunner, L. W. Molenkamp, K. Miyamoto, M. Arita, K. Shimada, T. Okuda, J. Kirschner, C. Tusche, H. Ebert, J. Minár, and F. Reinert, *Physical Review B* **103**, L161107 (2021).

[13] M. Ünzelmann, H. Bentmann, T. Figgemeier, P. Eck, J. N. Neu, B. Geldiyev, F. Diekmann, S. Rohlf, J. Buck, M. Hoesch, M. Kalläne, K. Rossnagel, R. Thomale, T. Siegrist, G. Sangiovanni, D. D. Sante, and F. Reinert, *Nature Communications* **12**, 3650 (2021).

[14] J. Schusser, H. Bentmann, M. Ünzelmann, T. Figgemeier, C.-H. Min, S. Moser, J. N. Neu, T. Siegrist, and F. Reinert, *Physical Review Letters* **129**, 246404 (2022).

[15] R. Ono, A. Marmodoro, J. Schusser, Y. Nakata, E. F. Schwier, J. Braun, H. Ebert, J. Minár, K. Sakamoto, and P. Krüger, *Physical Review B* **103**, 125139 (2021).

[16] M. Fanciulli, H. Volfová, S. Muff, J. Braun, H. Ebert, J. Minár, U. Heinzmann, and J. H. Dil, *Physical Review Letters* **118**, 067402 (2017).

[17] C.-H. Min, H. Bentmann, J. N. Neu, P. Eck, S. Moser, T. Figgemeier, M. Ünzelmann, K. Kissner, P. Lutz, R. J. Koch, C. Jozwiak, A. Bostwick, E. Rotenberg, R. Thomale, G. Sangiovanni, T. Siegrist, D. Di Sante, and F. Reinert, *Physical Review Letters* **122**, 116402 (2019).

[18] T. Figgemeier, M. Ünzelmann, P. Eck, J. Schusser, L. Crippa, J. Neu, B. Geldiyev, P. Kagerer, J. Buck, M. Kalläne, M. Hoesch, K. Rossnagel, T. Siegrist, L.-K. Lim, R. Moessner, G. Sangiovanni, D. Di Sante, F. Reinert, and H. Bentmann, *Physical Review X* **15**, 011032 (2025).

[19] S. S. Brinkman, X. L. Tan, B. Brekke, A. C. Mathisen, Ø. Finnseth, R. J. Schenk, K. Hagiwara, M.-J. Huang, J. Buck, M. Kalläne, M. Hoesch, K. Rossnagel, K.-H. Ou Yang, M.-T. Lin, G.-J. Shu, Y.-J. Chen, C. Tusche, and H. Bentmann, *Physical Review Letters* **132**, 196402 (2024).

[20] M. Schüler, U. D. Giovannini, H. Hübener, A. Rubio, M. A. Sentef, and P. Werner, *Science Advances* **6**, eaay2730 (2020).

[21] S. Cho, J.-H. Park, J. Hong, J. Jung, B. S. Kim, G. Han, W. Kyung, Y. Kim, S.-K. Mo, J. D. Denlinger, J. H. Shim, J. H. Han, C. Kim, and S. R. Park, *Phys. Rev. Lett.* **121**, 186401 (2018).

[22] S. Cho, J.-H. Park, S. Huh, J. Hong, W. Kyung, B.-G. Park, J. D. Denlinger, J. H. Shim, C. Kim, and S. R. Park, *Scientific Reports* **11**, 1684 (2021).

[23] R. Takahashi and N. Nagaosa, *Phys. Rev. B* **91**, 245133 (2015).

[24] J. Erhardt, C. Schmitt, P. Eck, M. Schmitt, P. Keßler, K. Lee, T. Kim, C. Cacho, I. Cojocariu, D. Baranowski, V. Feyer, L. Veyrat, G. Sangiovanni, R. Claessen, and S. Moser, *Phys. Rev. Lett.* **132**, 196401 (2024).

[25] M. Kang, S. Kim, Y. Qian, P. M. Neves, L. Ye, J. Jung, D. Puntel, F. Mazzola, S. Fang, C. Jozwiak, A. Bostwick, E. Rotenberg, J. Fuji, I. Vobornik, J.-H. Park, J. G. Checkelsky, B.-J. Yang, and R. Comin, *Nature Physics* **21**, 110 (2025).

[26] O. Fedchenko, K. Medjanik, S. Chernov, D. Kutnyakhov, M. Ellguth, A. Oelsner, B. Schönhense, T. R. F. Peixoto, P. Lutz, C.-H. Min, F. Reinert, S. Däster, Y. Acremann, J. Viehhaus, W. Wurth, J. Braun, J. Minár, H. Ebert, H. J. Elmers, and G. Schönhense, *New Journal of Physics* **21**, 013017 (2019).

[27] E. E. Krasovskii, V. N. Strocov, N. Barrett, H. Berger, W. Schattke, and R. Claessen, *Phys. Rev. B* **75**, 045432 (2007).

[28] V. N. Strocov, L. L. Lev, F. Alarab, P. Constantinou, X. Wang, T. Schmitt, T. J. Z. Stock, L. Nicolai, J. Očenášek, and J. Minár, *Nature Communications* **14**, 4827 (2023).

[29] R. P. Day, B. Zwartsenberg, I. S. Elfmov, and A. Damascelli, *npj Quantum Materials* **4**, 54 (2019).

[30] Y. Yen, G. Parusa, and M. Schüler, *First-principle tight-binding approach to angle-resolved photoemission spectroscopy simulations: importance of light-matter gauge and ubiquitous interference effects* (2024), arXiv:2402.14496 [cond-mat].

[31] U. De Giovannini, D. Varsano, M. A. L. Marques, H. Appel, E. K. U. Gross, and A. Rubio, *Physical Review A* **85**, 062515 (2012).

[32] U. De Giovannini, G. Brunetto, A. Castro, J. Walkenhorst, and A. Rubio, *ChemPhysChem* **14**, 1363 (2013).

[33] U. De Giovannini, H. Hübener, and A. Rubio, *Journal of Chemical Theory and Computation* **13**, 265 (2017).

[34] H. Ebert, D. Ködderitzsch, and J. Minár, *Reports on Progress in Physics* **74**, 096501 (2011).

[35] P. J. Feibelman and D. E. Eastman, *Phys. Rev. B* **10**, 4932 (1974).

[36] G. D. Mahan, *Phys. Rev. B* **2**, 4334 (1970).

[37] J. B. Pendry, *Surface Science* **57**, 679 (1976).

[38] M. Nozaki and P. Krüger, *Physical Review B* **110**, 195406 (2024).

[39] J. H. Ryoo and C.-H. Park, *Physical Review Letters* **135**, 056403 (2025).

[40] S. Hüfner, S. Schmidt, and F. Reinert, *Nuclear Instruments and Methods in Physics Research Section A: Accelerators, Spectrometers, Detectors and Associated Equipment Proceedings of the Workshop on Hard X-ray Photoelectron Spectroscopy*, **547**,

8 (2005).

[41] The surface of bulk three-dimensional systems can be modeled by slab geometries that are periodic in two dimensions.

[42] E. E. Krasovskii and W. Schattke, *Physical Review B* **56**, 12874 (1997).

[43] E. Krasovskii, *Nanomaterials* **12**, 10.3390/nano12224040 (2022).

[44] P. Borghetti, J. Lobo-Checa, E. Goiri, A. Mugarza, F. Schiller, J. Enrique Ortega, and E. E. Krasovskii, *Journal of Physics: Condensed Matter* **24**, 395006 (2012).

[45] E. E. Krasovskii and W. Schattke, *Phys. Rev. B* **59**, R15609 (1999).

[46] E. Krasovskii, *Nanomaterials* **11**, 10.3390/nano11051212 (2021).

[47] C. J. Joachain, *Quantum collision theory* (North-Holland, Amsterdam, The Netherlands, 1975).

[48] For semi-infinite systems, $f_{k,G}(z) \rightarrow 0$ as $z \rightarrow -\infty$.

[49] B. R. Johnson, *The Journal of Chemical Physics* **69**, 4678 (1978).

[50] G. Parusa, S. Fragkos, S. Beaulieu, and M. Schüller, Supplementary Material for “Accurate and efficient simulation of photoemission spectroscopy via Kohn-Sham scattering states” (2025).

[51] I. Gierz, M. Lindroos, H. Höchst, C. R. Ast, and K. Kern, *Nano Letters* **12**, 3900 (2012).

[52] M. J. v. Setten, M. Giantomassi, E. Bousquet, M. J. Verstraete, D. R. Hamann, X. Gonze, and G.-M. Rignanese, *Computer Physics Communications* **226**, 39 (2018).

[53] D. Vanderbilt, *Physical Review B* **41**, 7892 (1990).

[54] M. Schlipf and F. Gygi, *Computer Physics Communications* **196**, 36 (2015).

[55] We use the velocity operator $\hat{\Delta} = i[\hat{H}^{\text{KS}}, \hat{\mathbf{r}}]$.

[56] S. Fragkos, Q. Courtade, O. Tkach, J. Gaudin, D. Descamps, G. Barrette, S. Petit, G. Schönhense, Y. Mairesse, and S. Beaulieu, *Review of Scientific Instruments* **96**, 115201 (2025).

[57] S. Beaulieu, J. Schusser, S. Dong, M. Schüller, T. Pincelli, M. Dendzik, J. Maklar, A. Neef, H. Ebert, K. Hricovini, M. Wolf, J. Braun, L. Rettig, J. Minár, and R. Ernstorfer, *Phys. Rev. Lett.* **125**, 216404 (2020).

[58] S. Moser, *Journal of Electron Spectroscopy and Related Phenomena* **262**, 147278 (2023).

[59] C. S. Kern, A. Haags, L. Egger, X. Yang, H. Kirschner, S. Wolff, T. Seyller, A. Gottwald, M. Richter, U. De Giovannini, A. Rubio, M. G. Ramsey, F. C. Bocquet, S. Soubatch, F. S. Tautz, P. Puschnig, and S. Moser, *Physical Review Research* **5**, 033075 (2023).

[60] Y. Yen, J. A. Krieger, M. Yao, I. Robredo, K. Manna, Q. Yang, E. C. McFarlane, C. Shekhar, H. Borrman, S. Stoltz, R. Widmer, O. Gröning, V. N. Strocov, S. S. P. Parkin, C. Felser, M. G. Vergniory, M. Schüller, and N. B. M. Schröter, *Nature Physics* **20**, 1912 (2024).

[61] H. Boban, M. Qahosh, X. Hou, T. Sobol, E. Beyer, M. Szczepanik, D. Baranowski, S. Mearini, V. Feyer, Y. Mokrousov, Y. Zhou, Y. Su, K. Jin, T. Wichmann, J. Martinez-Castro, M. Ternes, F. S. Tautz, F. Lüpke, C. M. Schneider, J. Henk, and L. Plucinski, *Physical Review B* **111**, 115127 (2025).

[62] E. Bosoni, L. Beal, M. Bercx, P. Blaha, S. Blügel, J. Bröder, M. Callsen, S. Cottenier, A. Degomme, V. Dikan, K. Eimre, E. Flage-Larsen, M. Fornari, A. Garcia, L. Genovese, M. Giantomassi, S. P. Huber, H. Janssen, G. Kastlunger, M. Krack, G. Kresse, T. D. Kühne, K. Lejaeghere, G. K. H. Madsen, M. Marsman, N. Marzari, G. Michalicek, H. Mirhosseini, T. M. A. Müller, G. Petretto, C. J. Pickard, S. Poncé, G.-M. Rignanese, O. Rubel, T. Ruh, M. Sluydts, D. E. P. Vanpoucke, S. Vijay, M. Wolloch, D. Wortmann, A. V. Yakutovich, J. Yu, A. Zadoks, B. Zhu, and G. Pizzi, *Nature Reviews Physics* **6**, 45 (2024).

[63] G. Onida, L. Reining, and A. Rubio, *Reviews of Modern Physics* **74**, 601 (2002).

[64] C. S. Kern, A. Windischbacher, and P. Puschnig, *Physical Review B* **108**, 085132 (2023).

[65] J. K. Freericks, H. R. Krishnamurthy, and T. Pruschke, *Physical Review Letters* **102**, 136401 (2009).

[66] M. Schüller and M. A. Sentef, *Journal of Electron Spectroscopy and Related Phenomena* **253**, 147121 (2021).

[67] Y.-G. Choi, D. Jo, K.-H. Ko, D. Go, K.-H. Kim, H. G. Park, C. Kim, B.-C. Min, G.-M. Choi, and H.-W. Lee, *Nature* **619**, 52 (2023).

[68] M. Merboldt, M. Schüller, D. Schmitt, J. P. Bange, W. Bennecke, K. Gadge, K. Pierz, H. W. Schumacher, D. Momeni, D. Steil, S. R. Manmana, M. A. Sentef, M. Reutzel, and S. Mathias, *Nature Physics* **21**, 1093 (2025).